Progress In Electromagnetics Research, Vol. 131, 391–407, 2012

A THREE DIMENSIONAL ANALYTICAL CALCULATION OF THE AIR-GAP MAGNETIC FIELD AND TORQUE OF COAXIAL MAGNETIC GEARS

Y.-J. Ge*, C.-Y. Nie, and Q. Xin

School of Mechanical Engineering, Dalian Jiaotong University, Dalian 116028, China

Abstract—In order to solve the defects that the end-effect of magnetic field is ignored in two dimension (2-D) analytical method or 2-D finite element method (FEM); meanwhile, mass computer resource and time for parametric design or optimization are wasted in three dimension (3-D) FEM, a concise and efficient 3-D analytical approach is put forward for the calculation of the air-gap magnetic field and torque of coaxial magnetic gears. Based on the cylindrical coordinates where a coaxial magnetic gear is in, the equivalent current model and vector magnetic potential equation of permanent magnets in high speed permanent magnetic ring are constituted. By superposed magnetic flux density of every tile permanent magnets on high speed permanent magnetic ring in cylindrical coordinates, a air-gap magnetic field 3-D analytical formula is set up without ferromagnetic pole-pieces; in the interest of modulated air-gap magnetic field 3-D analytical formula with ferromagnetic pole-pieces, three types boundary conditions using state equations of contact surfaces between ferromagnetic pole-pieces and air-gap are established by a thorough analysis of the modulate mechanism of ferromagnetic pole-pieces. Finally, magnets of the low speed permanent magnetic ring are reduced to a distribution of equivalent current, which experience the Lorentz force in modulated magnetic field of high speed permanent magnetic ring for torque calculation. The integrals in all aforementioned calculation are axial, so the end-effect is embodied in above analytical model and more precise than 2-D analytical method or 2-D FEM. As the calculation results, the formula is accurate but faster than the 3-D FEM. The analytical model is suited for programmable calculation and that will make the structural and parametric design or optimization of coaxial magnetic gears simple and timesaving.

Received 11 July 2012, Accepted 30 August 2012, Scheduled 17 September 2012

* Corresponding author: Yanjun Ge (yjge@djtu.edu.cn).

1. INTRODUCTION

Coaxial magnetic gear (CMG) is a novel magnetic transmission device with coaxial inner and outer rotor, whose principle of operation was introduced in [1]. It employs rare-earth permanent magnets on both the inner and the outer rotor, and it has ferromagnetic pole-pieces between the two rotors. The air-gap magnetic field between rotors is modulated by the ferromagnetic pole-pieces. Meanwhile, the gear ratio is achieved.

The pole number of magnets on high speed rotor is less than the low speed one in CMGs. Both of them produce magnetic field in the air-gap, and this field is modulated by the ferromagnetic pole-pieces which have alternated ferromagnetic and non-ferromagnetic pole-pieces. Because the efficient utilization of all the permanent magnets of the inner and the outer rotor contribute to torque transmitting, the air-gap magnetic flux density and torque density are higher than those of traditional magnetic gears [1] and can be used in many aspects of our life [2, 3].

The performance of air-gap magnetic field and torque play a pivotal role in permanent magnetic gears. An exact calculation of them is vitally important for their design and optimization [4–7]. The common method for magnetic field calculation is either analytical method or numerical method (especially the finite element method, FEM) [6–10]. The CMGs have two air-gaps between the inner and the outer rotor which are isolated by ferromagnetic pole-pieces. Moreover, the ferromagnetic pole-pieces are made by alternated ferromagnetic and non-ferromagnetic pole-pieces. Therefore, the two air-gap magnetic fields are modulated by the ferromagnetic pole-pieces that the magnetic field will be aberrantly nonlinear and the amount of its corresponding space harmonic spectrums will be changed. So the analytical model may be very difficult to set up for above reasons. Based on the magnetic field integral method and the equivalent current model, literature [11, 12] derived torque calculation formula for permanent magnetic gear with parallel axis. But their methods are inappropriate for the CMGs on account of the lack of ferromagnetic pole-pieces to impact the air-gap magnetic field. Recently, some researchers have calculated and investigated the characteristics of ferromagnetic material and antiferromagnetic structures according to the complex numerical methods [13, 14]. Based on the Poisson's and Laplace's equation, literature [15, 16] obtained a two dimension (2-D) analytical result of air-gap magnetic field for CMGs. They used separation of variables method by the boundary conditions about permanent magnets, air-gaps, and ferromagnetic pole-pieces.

At present, the analysis or calculation about CMGs is mainly 2-D FEM [17–19], since it is simpler and faster than the three dimension (3-D) FEM.

The magnetic flux density is different along the axis, especially when the field point is on the end of the axis. This is called magnetic field end-effect which has been neglected in 2-D analytical method or 2-D FEM. It supposes that air-gap magnetic fields are invariable along the axis, and will produce great error in calculation results when length/radius ratio of permanent magnet is low [20, 21]. From the experiment results, literature [22] validated that error between 2-D FEM and test is 30%–40%. So it is essential to calculate the air-gap magnetic field and torque by 3-D method.

Literature [22] used 3-D FEM to analyze and calculate the CMGs by scalar magnetic potential. The calculation results agreed with the measured ones basically. With 3-D FEM, literature [23] also investigated the influence of design parameters on the air-gap magnetic flux density and torque capacity of CMGs, and it is a guide for structural parameter design or optimization about CMGs. The cogging torque of CMGs is also studied in literature [24, 25] and validated by tests.

3-D FEM wastes mass computer memory resource and CPU time for dividing grids and nodes, though it is more precise. Moreover, there are some defects in FEM calculation for permanent magnetic gear: (1) the geometrical size and material character must be well-defined beforehand for the calculated object, and they can not be changed when FEM program is calculating, so that is not flexible in design. (2) 3-D FEM can offer neither closed-form solution nor detailed model parameters, and it is tentative in parametric optimization based on single step [5].

Because of the 3-D analysis and calculation about electromagnetics is much complicated, there is no published literature for 3-D analytical method about CMGs.

CMGs have two transmission modes: (1) ferromagnetic pole-pieces are fixed, high and low speed permanent magnet ring rotate in opposite direction. This is called the negative accelerated/decelerated device; (2) low speed permanent magnet ring is fixed, high speed permanent magnet ring and ferromagnetic pole-pieces rotate in same direction. This is called the positive accelerated/decelerated device. The former will be studied in this paper by 3-D analysis, and the calculation method here for air-gap magnetic field and torque is also suited to the latter one.

To avoid the great calculation error in 2-D analysis and to take magnetic flux leak and end-effect into account, we choose cylindrical

coordinates for 3-D analytical calculation of the air-gap magnetic field and torque of CMGs. Firstly, a vector magnetic potential equation of air-gap magnetic field without ferromagnetic pole-pieces is evaluated according to the equivalent current model of permanent magnet, and the 3-D analytical model of magnetic flux density in air-gap is gained by superposing single one that produced by each tile permanent magnet. Then, from the modulating mechanism, boundary conditions (including the magnetic flux leak between poles when magnetic lines close in the ferromagnetic pole-pieces) are obtained on surfaces between air-gap and ferromagnetic pole-pieces. And from these boundary conditions, the 3-D air-gap magnetic field analytical model is constituted with the modulating mechanism of ferromagnetic pole-pieces. Finally, to calculate the torque, magnets of the low speed permanent magnetic ring are reduced to a distribution of equivalent current, which experiences the Lorentz force in modulated magnetic field of high speed permanent magnetic ring. Because of all the integrals are along the axial of permanent magnetic ring, the end-effect is taken into account in the constituted model of this paper.

Because of the magnetic flux leak and end-effect are considered in above analysis and calculation, the constituted model is more precise than 2-D analytical method or 2-D FEM. Compared with 3-D FEM, the analytical method is suited for programmable calculation and that will make the structural parameter design or optimization of CMGs simple and timesaving. It eliminates the blindfold defect of 3-D FEM in trial method with mass computer resource and time, also adapts to the parameterized and the serial applications in technical projects.

2. CALCULATION OF MAGNETIC FIELD OF HIGH SPEED PERMANENT MAGNETIC RING WITHOUT FERROMAGNETIC POLE-PIECES

Figure 1 shows the topology of a typical coaxial magnetic gear. The high speed permanent magnetic ring (inner rotor), low speed permanent magnetic ring (outer rotor), and the ferromagnetic pole-pieces rotate around common-axis. And their radii are $R_i(1)$, $R_i(2)$, $R_o(1)$, $R_o(2)$, $R_m(1)$, and $R_m(2)$ respectively. Their corresponding edge angles of tile permanent magnets in the inner rotor, ferromagnetic pole-pieces, and the outer rotor are $\phi_i(1)$, $\phi_i(2)$, $\phi_m(1)$, $\phi_m(2)$, $\phi_o(1)$, and $\phi_o(2)$ respectively. The $\phi_i(1)$, $\phi_m(1)$, and $\phi_o(1)$ overlap with x-axis. φ is circumferential angle, and $\boldsymbol{\rho}$ is radial vector which starts from point O as shown in Figure 1(a).

Because z-axial length of two rotors and the ferromagnetic pole-pieces may be different, their coordinates are denoted by $Z_i(1)$, $Z_i(2)$,

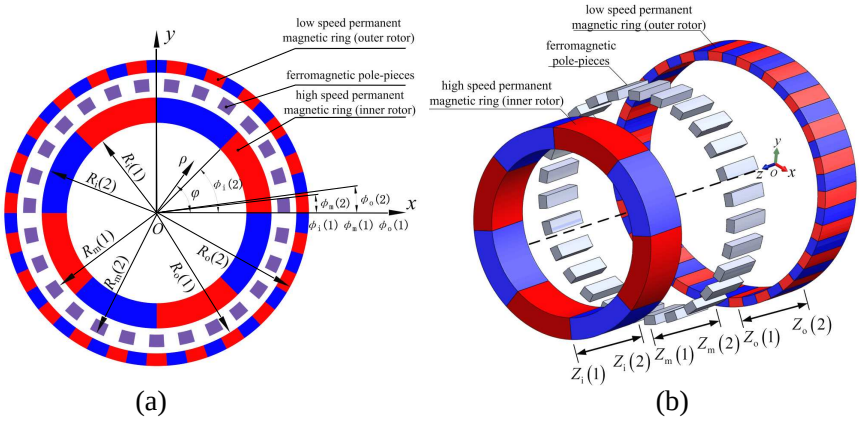

Figure 1. Field modulated permanent magnetic gear. (a) Cross section of the considered magnetic gear. (b) Exploded view.

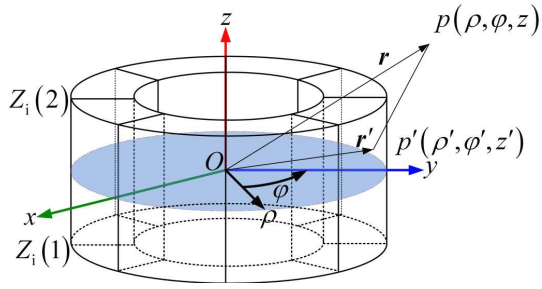

Figure 2. Permanent magnets on the inner rotor in cylindrical coordinates system.

$Z_o(1)$, $Z_o(2)$, $Z_m(1)$, and $Z_m(2)$ respectively as shown in Figure 1(b).

Figure 2 is the inner rotor of Figure 1 in cylindrical coordinates system. The origin O, the same as the one showed in Figure 1, locates in the center of cylinder of inner rotor. The unit vectors of the cylindrical coordinates along ρ, φ, and z are $\mathbf{e}_\rho$, $\mathbf{e}_\varphi$, and $\mathbf{e}_z$ respectively. A source point coordinate and a field point coordinate of a random permanent magnet in Figure 2 are $p'(\rho', \varphi', z')$ and p (ρ, φ, z) respectively. Their corresponding radius vectors are $\mathbf{r}'$ and $\mathbf{r}$ respectively.

In the cylindrical coordinates system, supposed $\mathbf{B}$ is magnetic flux density in a random field point of air-gap, and its corresponding vector

potential is $\mathbf{A}$. It can be expressed as

$$\begin{aligned}\mathbf{B}&=\nabla\times\mathbf{A}=\mathbf{e}_\rho B_\rho+\mathbf{e}_\varphi B_\varphi+\mathbf{e}_z B_z\\&=\mathbf{e}_\rho\left(\frac{1}{\rho}\frac{\partial A_z}{\partial\varphi}-\frac{\partial A_\varphi}{\partial z}\right)+\mathbf{e}_\varphi\left(\frac{\partial A_\rho}{\partial z}-\frac{\partial A_z}{\partial\rho}\right)+\mathbf{e}_z\left(\frac{\partial}{\partial\rho}(\rho A_\varphi)-\frac{\partial A_\rho}{\partial\varphi}\right)\end{aligned}$$

Supposed $\mathbf{B}_\Omega$ is magnetic flux density in a random field point p (ρ, φ, z) of air-gap, and its modulus along ρ orientate in the cylindrical coordinate system is $B_{\Omega\rho}$. Because only the component $B_{\Omega\rho}\mathbf{e}_\rho$ of $\mathbf{B}_\Omega$ in the cylindrical coordinate system along ρ orientate contributes to the torque, so the analytical formula is just about $B_{\Omega\rho}$ in this paper. By the method of magnetic field calculation in literature [26] gives

$$B_{\Omega\rho}=|\mathbf{B}_\Omega|=|B_{\Omega\rho}\mathbf{e}_\rho|=\frac{\mu_0 M}{4\pi}\sum_{n_i=1}^{N_i}\sum_{j=1}^{2}\sum_{k=1}^{2}(-1)^{(s+1+j+k)}\left\{\begin{array}{l}\Delta\rho'\sum\limits_{n=0}^{N_{\rho'}} S_{\rho'}(n)\,\rho'(n)\sin(\varphi-\phi_i(j))\\ \quad\cdot I_1(\rho,\varphi,z;\rho'(n),\phi_i(j),Z_i(k))\\ +\Delta\varphi'\sum\limits_{m=0}^{N_{\varphi'}} S_{\varphi'}(m)(z-Z_i(j))\cos(\varphi-\varphi'(m))\\ \quad\cdot I_2(\rho,\varphi,z;R_i(k),\varphi'(m),Z_i(j))\end{array}\right\}\tag{1}$$

In (1), $S_{\rho'}(n)$ and $S_{\varphi'}(m)$ are Simpson's coefficients. I_1 and I_2 can be gained from the following equations.

$$\sum_{k=1}^{2}(-1)^{k+1}I_1\left(\rho,\varphi,z;\rho',\varphi',z_i(k)\right)=\int_{Z_i(1)}^{Z_i(2)}g^3\left(\rho,\varphi,z;\rho',\varphi',z'\right)dz'$$

$$\sum_{k=1}^{2}(-1)^{k+1}I_2\left(\rho,\varphi,z;R_i(k),\varphi',z'\right)=\int_{R_i(1)}^{R_i(2)}g^3\left(\rho,\varphi,z;\rho',\varphi',z'\right)\rho'd\rho'$$

where

$$g\left(\rho,\varphi,z;\rho',\varphi',z'\right)=\frac{1}{|\mathbf{r}-\mathbf{r}'|}=\frac{1}{\sqrt{\rho^2+\rho'^2-2\rho\rho'\cos(\varphi-\varphi')+(z-z')^2}}$$

3. MODULATED MECHANISM AND BOUNDARY CONDITIONS OF FERROMAGNETIC POLE-PIECES

$\mathbf{B}$ is changed after installed ferromagnetic pole-pieces between the inner and the outer rotor, for $\mathbf{B}$ and its corresponding $\mathbf{A}$ embodies some boundary conditions as shown in Figure 3.

Supposed vector potential $\mathbf{A}_1$, $\mathbf{A}_2$, and $\mathbf{A}_3$ are denoted to the radial, angular, and axial interface of ferromagnetic pole-pieces

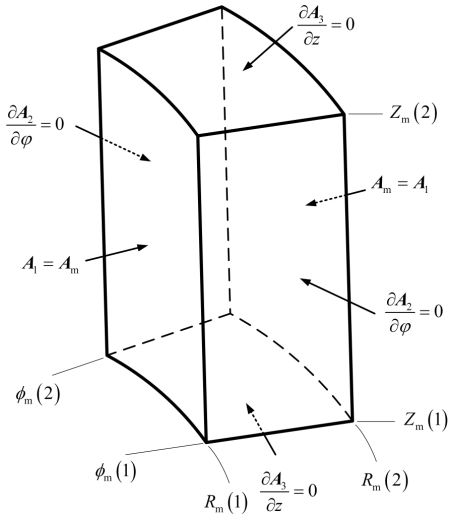

Figure 3. Boundary conditions of ferromagnetic pole-pieces.

marched with the air-gap, and $\mathbf{A}_m$ is inside ferromagnetic pole-pieces. According to the boundary conditions of static magnetic field, we have:

(a) The vertical component of magnetic flux density is continuous along radial interface, so the first-type boundary condition in air-gap of modulated magnetic field is

$$\mathbf{A}_1 = \mathbf{A}_m \begin{pmatrix} \rho = R_m(1) \text{ or } \rho = R_m(2) \\ \phi_m(1) \le \varphi \le \phi_m(2) \\ Z_m(1) \le z \le Z_m(2) \end{pmatrix} \tag{2}$$

(b) Because of the great permeability of ferromagnetic pole-pieces [27]; besides the magnetization is uniform along radius and vertical with the sectored interfaces, these sectored interfaces are isopotential surface approximately, namely $\mathbf{A}_2$ is not changed along sector angular direction [5, 16]. So the second-type boundary condition in air-gap of modulated magnetic field is

$$\frac{\partial \mathbf{A}_2}{\partial \varphi} = 0 \begin{pmatrix} R_m(1) \le \rho \le R_m(2) \\ \varphi = \phi_m(1) \text{ or } \varphi = \phi_m(2) \\ Z_m(1) \le z \le Z_m(2) \end{pmatrix} \tag{3}$$

In (3), ferromagnetic pole-pieces has N_m segments and their edge angles are

$$\phi_m(1) = \frac{2\pi}{N_m}(n_m - 1), \quad \phi_m(2) = \frac{2\pi}{N_m} n_m, \quad (n_m = 1, 3, \ldots, N_m - 1)$$

(c) In the same way, $\mathbf{A}_3$ is not changed along axial direction on the axial interfaces, because we only calculate $B_{\Omega\rho}$ here. So the third-type boundary condition is

$$\frac{\partial \mathbf{A}_3}{\partial z} = 0 \begin{pmatrix} R_m(1) \le \rho \le R_m(2) \\ \phi_m(1) \le \varphi \le \phi_m(2) \\ z = Z_m(1) \text{ or } z = Z_m(2) \end{pmatrix} \tag{4}$$

From the first-type boundary condition: magnetic flux density is not changed through the two arc surfaces of ferromagnetic pole-pieces, and namely the magnetic field produced by permanent magnets is shifted from inner radius of ferromagnetic pole-pieces to outer constantly. If the thickness of ferromagnetic pole-pieces is $\Delta\rho_m = R_m(2) - R_m(1)$, then magnetic flux density keeps constant in this range. The magnetic flux density $B_{\Omega\rho 1}$ at $p\ (\rho,\ \varphi,\ z)$ will be invariable and it is equal with $B_{\Omega\rho}$ at $p\,(\rho - \Delta\rho_m, \phi, z)$. Because of this, substituting $\rho = \rho - \Delta\rho_m$ into (1), it yields

$$B_{\Omega\rho 1}\,(\rho, \varphi, z) = B_{\Omega\rho}\,(\rho - \Delta\rho_m, \varphi, z) \tag{5}$$

From the second-type boundary condition: we find that

$$\frac{\partial A_\rho}{\partial \varphi} = 0, \quad \frac{\partial A_\varphi}{\partial \varphi} = 0, \quad \frac{\partial A_z}{\partial \varphi} = 0$$

At point $p\ (\rho,\ \varphi,\ z)$, magnetic flux density $B_{\Omega\rho 2}$ is supposed as the radial component of whole permanent magnets on the inner rotor and it satisfies the second-type boundary condition. Then (1) can be rewritten as

$$B_{\Omega\rho 2} = \frac{\mu_0 M}{4\pi} \sum_{n_i=1}^{N_i} \sum_{j=1}^{2} \sum_{k=1}^{2} (-1)^{(s+1+j+k)} \left[\Delta\varphi' \sum_{m=0}^{N_{\varphi'}} S_{\varphi'}(m)(z - Z_i(j)) \cos\big(\varphi - \varphi'(m)\big) I_2\big(\rho, \varphi, z; R_i(k), \varphi'(m), Z_i(j)\big) \right] \tag{6}$$

In the same way, from the third-type boundary condition, at point $p\ (\rho, \varphi, z)$, magnetic flux density $B_{\Omega\rho 3}$ is the radial component of whole permanent magnets on the inner rotor and it satisfies the third-type boundary condition. It yields

$$B_{\Omega\rho 3} = \frac{\mu_0 M}{4\pi} \sum_{n_i=1}^{N_i} \sum_{j=1}^{2} \sum_{k=1}^{2} (-1)^{(s+1+j+k)} \left[\Delta\rho' \sum_{n=0}^{N_{\rho'}} S_{\rho'}\,(n)\, \rho'\,(n) \sin\left(\varphi - \phi_i\,(j)\right) I_1\left(\rho, \varphi, z; \rho'\,(n)\,, \phi_i\,(j)\,, Z_i\,(k)\right) \right] \tag{7}$$

Table 1. Parameters of analytical calculation.

inner rotor		ferromagnetic pole-pieces		outer rotor	
symbol	value	symbol	value	symbol	value
N_i	4	N_m	54	N_o	46
$R_i(1)$	54 mm	$R_m(1)$	69 mm	$R_o(1)$	76 mm
$R_i(2)$	68 mm	$R_m(2)$	75 mm	$R_o(2)$	82 mm
$\phi_i(1)$	$\frac{2\pi}{N_i}(n_i-1)$	$\phi_m(1)$	$\frac{2\pi}{N_m}(n_m-1)$	$\phi_o(1)$	$\frac{2\pi}{N_o}(n_o-1)$
$\phi_i(2)$	$\frac{2\pi n_i}{N_i}$	$\phi_m(2)$	$\frac{2\pi n_m}{N_m}$	$\phi_o(2)$	$\frac{2\pi n_o}{N_o}$
L_i	14 mm	L_m	14 mm	L_o	14 mm
$Z_i(1)$	$-\frac{L_i}{2}$	$Z_m(1)$	$-\frac{L_m}{2}$	$Z_o(1)$	$-\frac{L_o}{2}$
$Z_i(2)$	$\frac{L_i}{2}$	$Z_m(2)$	$\frac{L_m}{2}$	$Z_o(2)$	$\frac{L_o}{2}$

Using parameters in Table 1, (1), (5), (6), and (7) are programmed with Matlab 7. The magnets used for CMGs are sintered Nd-Fe-B material, and their magnetizations are all $M = 890000$ (A/m).

Along the radius $R_o(1)$ and $R_i(2)$, divide up the surface of cylindrical air-gap into 360 segmentations (the air-gap magnetic field of the outer rotor can be calculated according replacing parameters whose subscript is i by the ones of o). With the constituted model of this paper, $B_{\Omega\rho}$ is calculated when φ increased by each one degree as shown in Figure 1 on a 3.0 GHz computer which has quad-core CPU and 2 GB memory. The results are shown in Figure 4(a) to Figure 4(d).

It takes approximately 15 s respectively to compute of air-gap magnetic field at $R_o(1)$ of the inner rotor and at $R_i(2)$ of the outer rotor, as shown in Figure 4(a) and Figure 4(b). The Figure 4(c) takes 20 s. The same parameters as Table 1 are checked with the same computer using the Maxwell 3-D Field Simulator from Ansoft 14, and it takes approximately 25 min respectively for the analysis not including modeling, meshing, setup and postprocess in Figure 4(a) or Figure 4(b).

For distinctly explaining the results, a main waveform in Figure 4(a) and Figure 4(b) is chosen.

From Figure 4(a), we find: the radial component of the air-gap magnetic field produced by the inner permanent magnets is entire sinusoid curve without ferromagnetic pole-pieces; when the ferromagnetic pole-pieces is installed, the eight main waveform is modulated, and a modulated harmonic wave is formed along the ferromagnetic pole-pieces covered by sectored edge angle of permanent magnets. The curve of the constituted model of this paper is almost the same as the one of FEM according to Figure 4(a).

The wave crest and trough in region I and II are the enhancement

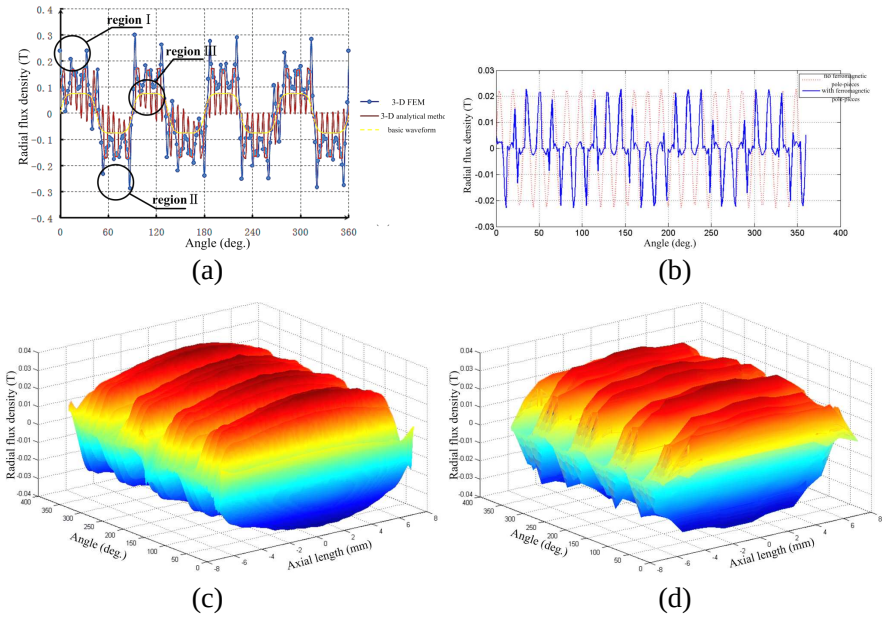

Figure 4. Flux density distribution along the radial component. (a) Air-gap magnetic field at $R_o(1)$ produced by the inner rotor. (b) Air-gap magnetic field at $R_i(2)$ of the outer rotor. (c) 3-D curve of air-gap magnetic field at $R_o(1)$ of the inner rotor (constituted model). (d) 3-D curve of air-gap magnetic field at $R_o(1)$ of the inner rotor (FEM model).

of air-gap magnetic field which is produced by the inner rotor and modulated by the ferromagnetic pole-pieces. This is the invariable shift of magnetic flux density derived by the first-type boundary condition. The same curve which overlaps basic waveform is the air interval of ferromagnetic pole-pieces. The permeability in air-gap of these segments is not changed, so the magnetic flux density is not modulated. In addition, also from Figure 4(a), because of the second-type boundary condition in region III, the magnetic flux lines from permanent magnets go through angular edge of ferromagnetic pole-pieces and back to the adjacent permanent magnets, therefore a closed circuit is formed between ferromagnetic pole-pieces and permanent magnets, the magnetic energy does not be transferred from the inner rotor to the outer rotor (in the same way from the outer rotor to the inner rotor), and this closed circuit brings magnetic flux leak between magnetic poles. With the leak, magnetic flux density in air-gap is

decreasing, and these values are less than ones of basic waveform.

From Figure 4(b), we find: because of the large number of magnetic poles and high rotational frequency, the magnetic field waveform produced by the outer rotor is dense. Its harmonic spectrum is obvious enough to express the modulated effect of ferromagnetic pole-pieces. The wave crest and trough of magnetic flux densities in the region with non-ferromagnetic material of ferromagnetic pole-pieces are almost cut out entirely, only left the ones going through ferromagnetic pole-pieces. From Figure 4(b) the modulated magnetic field has distinct eight waveform and it is equal to the magnetic pole number of permanent magnets on the inner rotor; by the way gear ratio is accomplished. Because of a large number of magnetic pole and clear modulated effect in Figure 4(b), 3-D FEM curve is not drawn to avoid confusion. Its comparative result of the constituted model and 3-D FEM refer to Figure 4(a).

From Figure 4(c) and Figure 4(d), we find: when the angular and altitudinal coordinates are variable and the radius is constant, peak value of magnetic flux density occurs at axial middle plane on the rotor shaft, viz. $z = 0$. When this plane is closer to the end of the shaft, the magnetic flux density is less gradually. The minimum occurs at plane $Z_i(1) = -L_i/2$ and $Z_i(2) = L_i/2$, this is the end-effect. The length is less, the curvature is larger, and the end-effect is more obvious, it is through the third-type boundary condition that makes it. The curvilinear plane of the constituted model of this paper and 3-D FEM are alike as shown in Figure 4(c) and Figure 4(d).

4. TORQUE ANALYSIS OF OUTER ROTOR

Figure 5 is the equivalent current model of a tile permanent magnet on the outer rotor. The orientations about $\mathbf{J}_{ov}$ and $\mathbf{J}_{os}$ are determined by right-hand rule.

There are N_o tile permanent magnets on the outer rotor, and two surface current densities on each permanent magnet contribute to the torque transmission. For the initial position is zero (viz. an edge on tile permanent magnet overlaps with x-axis) such as Figure 1, the surface current of permanent magnet flows along the radial edge surface of

$$\phi_o(1) = 2\pi\,(n_o - 1)/N_o \quad (n_o = 1, 2, \ldots, N_o)$$

And

$$\phi_o(2) = 2\pi n_o/N_o \quad (n_o = 1, 2, \ldots, N_o)$$

When the outer rotor rotates an angle, its total volume current is

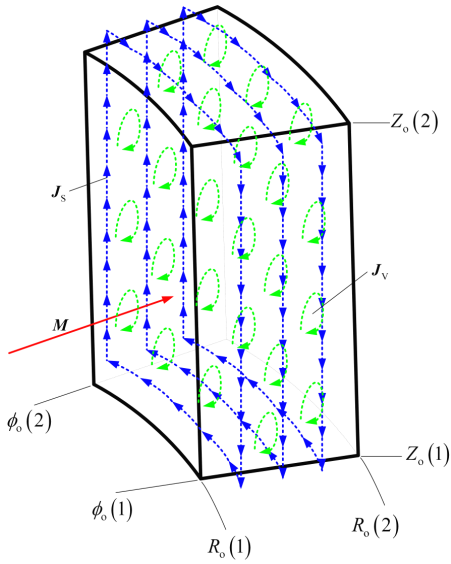

Figure 5. Equivalent current model of a tile permanent magnet on the outer rotor.

zero and its surface current [26] is

$$\mathbf{J}_{os} = \begin{cases} M \cdot \mathbf{e}_z \begin{pmatrix} R_o(1) \le \rho \le R_o(2) \\ \phi_o(2) = \alpha_{o0} + \frac{2\pi}{N_o} n_o \\ Z_o(1) \le z \le Z_o(2) \end{pmatrix} \\ -M \cdot \mathbf{e}_z \begin{pmatrix} R_o(1) \le \rho \le R_o(2) \\ \phi_o(1) = \alpha_{o0} + \frac{2\pi}{N_o} (n_o - 1) \\ Z_o(1) \le z \le Z_o(2) \end{pmatrix} \end{cases} \tag{8}$$

Supposed $\mathbf{T}$ is the torque of the outer rotor as showed in Figure 1, and in literature [26] it is given by

$$\mathbf{T} = \oint_s \mathbf{r}_o \times (\mathbf{J}_{os} \times \mathbf{B}_\Omega) ds \tag{9}$$

Substituting (8) and $B_{\Omega\rho}$ into (9), it yields

$$T(\alpha_{o0}) = 2M \sum_{n_o=1}^{N_o} (-1)^{n_o} \int_{Z_o(1)}^{Z_o(2)} \int_{R_o(1)}^{R_o(2)} \rho B_{\Omega\rho} d\rho dz \tag{10}$$

In (10), $B_{\Omega\rho}$ can be calculated by (1), (5), (6), and (7) according to the corresponding boundary condition. The coefficient $2M$ takes

into account the fact that there are two surface currents at the interface between neighboring tile permanent magnets, and these surface currents have the same orientation and function for torque calculation.

Rewriting (10) with Simpson's method, we have

$$T(\alpha_{o0}) = \frac{2ML_o\Delta\rho_o}{N_\rho N_z} \sum_{n_o=1}^{N_o} (-1)^{n_o} \sum_{p=0}^{N_z} S_z(p) \sum_{q=0}^{N_\rho} S_\rho(q)\, \rho(q)\, B_{\Omega\rho} \quad (11)$$

In (11), where $\Delta\rho_o = R_o(2) - R_o(1)$, and notice the integration points are

$$\rho(q) = R_o(1) + q\,(R_o(2) - R_o(1))/N_\rho, \quad (q = 0, 1, 2, \ldots, N_\rho)$$

And

$$z(p) = Z_o(1) + p\,(Z_o(2) - Z_o(1))/N_z, \quad (p = 0, 1, 2, \ldots, N_z)$$

$S_z(p)$ and $S_\rho(q)$ are integration coefficient respectively.

Equation (11) is programmed with the same parameters as Table 1. The torque is calculated for α_{o0} from 0° to 16°, (viz. the outer rotor rotates a pair of pole angle), as shown in Figure 6. In this figure 2-D and 3-D FEM are expressed in terms of discrete points.

From Figure 6, the values from the constituted model of this paper are almost comparable with 3-D FEM. The peak torque occurs when outer rotor rotates the angle of half pole, viz. α_{o0} is 0°, 8°, or 16°. The calculation speed by the constituted model of this paper is much faster than the 3-D FEM. It took approximately 1 h on a 3.0 GHz quad-core

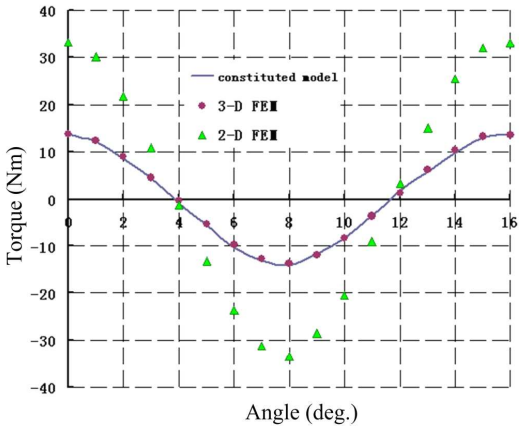

Figure 6. Torque T vs. angle α_{o0}.

CPU and 2 GB memory computer for 16 torque values. Meantime, the same data are computed on the same computer using 3-D FEM from Ansoft 14. It took approximately 5 h for the analysis not including modeling, meshing, setup and postprocessing.

Furthermore, the calculation speed of 2-D FEM is much fast (just 5 min) in Figure 6, however its end-effect of permanent magnets is neglected and the calculation results are 50% bigger than 3-D FEM. The constituted model of this paper is based on 3-D model and takes into account the end-effect and the magnetic flux leak between magnetic poles. And that it is also a better method to obtain the exact result.

5. CONCLUSION

(a) The end-effect of permanent magnets is neglected in 2-D analysis, so the calculation result of 2-D has bigger errors than 3-D, and there will be greater end-effect and errors in 2-D analysis when the length/radius ratio of permanent magnets is smaller. Because of all the integrals are along the axial of permanent magnetic ring, the end-effect is taken into account in the constituted model.

(b) Ferromagnetic pole-pieces is essential part in CMGs and its mechanical configuration and material character makes air-gap between the inner and the outer rotor forming three types boundary conditions: The first-type boundary condition is the invariable shift of magnetic flux density and enhances the wave crest and trough in the modulated region of basic waveform; The second-type makes the magnetic flux leak between poles and deduces air-gap magnetic flux density; The third-type forms the end-effect of permanent magnets.

(c) When the angular and altitudinal coordinates are variable and the radius is constant, the peak value of magnetic flux density is at the middle plane on the rotor shaft. It is less when the plane is closer to the end of the shaft. The minimum occurs at the two ends, the less the axial length is, the larger the curvature is in orientation, and more obvious the end-effect is.

(d) The second-type boundary condition makes magnetic flux leak between poles, and the third-type boundary condition produces end-effect, both of them will deduce the efficiency of CMGs. How to decrease the leak and the end-effect is the key work of CMGs for the future.

(e) Compared with 2-D analysis or 2-D FEM, the 3-D analysis is more precise because of embodying the end-effect. The constituted model of this paper is the same accurate in comparison with the 3-D FEM but much faster; moreover, the design parameters can be

replaced without re-constituting the model. Meanwhile the model is readily programmed and is ideal for parametric analysis. It should be of considerable use in the design and optimization of CMG devices.

ACKNOWLEDGMENT

This work was supported by Science and Technology Planning Project (Project No. 2010220004) of Liaoning Province, China.

REFERENCES

1. Atallah, K. and D. Howe, "A novel high-performance magnetic gear," *IEEE Trans. Magn.*, Vol. 37, No. 4, 2844–2846, Jul. 2001.
2. Jian, L. and K.-T. Chau, "Design and analysis of a magnetic-geared electronic-continuously variable transmission system using finite element method," *Progress In Electromagnetics Research*, Vol. 107, 47–61, 2010.
3. Jian, L., G. Xu, Y. Gong, J. Song, J. Liang, and M. Chang, "Electromagnetic design and analysis of a novel magnetic-gear-integrated wind power generator using time-stepping finite element method," *Progress In Electromagnetics Research*, Vol. 113, 351–367, 2011.
4. Jian, L., G. Xu, J. Song, H. Xue, D. Zhao, and J. Liang, "Optimum design for improving modulating-effect of coaxial magnetic gear using response surface methodology and genetic algorithm," *Progress In Electromagnetics Research*, Vol. 116, 297–312, 2011.
5. Jian, L. and K.-T. Chau, "Analytical calculation of magnetic field distribution in coaxial magnetic gears," *Progress In Electromagnetics Research*, Vol. 92, 1–16, 2009.
6. Babic, S. I. and C. Akyel, "Improvement in the analytical calculation of the magnetic field produced by permanent magnet rings," *Progress In Electromagnetics Research C*, Vol. 5, 71–82, 2008.
7. Ravaud, R., G. Lemarquand, V. Lemarquand, and C. Depollier, "The three exact components of the magnetic field created by a radially magnetized tile permanent magnet," *Progress In Electromagnetics Research,* Vol. 88, 307–319, 2008.
8. Ravaud, R., G. Lemarquand, V. Lemarquand, and C. Depollier, "Discussion about the analytical calculation of the magnetic field create by permanent magnets," *Progress In Electromagnetics Research B*, Vol. 11, 281–297, 2009.

9. Ravaud, R. and G. Lemarquand, "Magnetic couplings with cylindrical and plane air gaps: Influence of the magnet polarization direction," *Progress In Electromagnetics Research B*, Vol. 16, 333–349, 2009.
10. Ravaud, R. and G. Lemarquand, "Modelling an ironless loudspeaker by using three-dimensional analytical approach," *Progress In Electromagnetics Research*, Vol. 91, 53–68, 2009.
11. Furlani, E. P., "A two-dimensional analysis for the coupling of magnetic gears," *IEEE Trans. Magn.*, Vol. 33, No. 3, 2317–2321, May 1997.
12. Jørgensen, F. T., T. O. Andersen, and P. O. Rasmussen, "Two dimensional model of a permanent magnet spur gear," *IEEE Industry Applications Conference, Fortieth IAS Annual Meeting*, 261–265, Kowloon, Hong Kong, China, Oct. 2–6, 2005.
13. Wu, C.-J. and Y.-L. Chen, "Microwave properties of a high-temperature superconductor and ferromagnetic bilayer structure," *Progress In Electromagnetics Research*, Vol. 111, 433–445, 2011.
14. Tarkhanyan, R. H., "New class of surface magnon polaritons in enantiomeric antiferromagnetic structures," *Progress In Electromagnetics Research B*, Vol. 39, 55–69, 2012.
15. Lubin, T., S. Mezani, and A. Rezzoug, "Improved analytical model for surface-mounted PM motors considering slotting effects and armature reaction," *Progress In Electromagnetics Research B*, Vol. 25, 293–314, 2010.
16. Lubin, T., S. Mezani, and A. Rezzoug, "Analytical computation of the magnetic field distribution in a magnetic gear," *IEEE Trans. Magn.*, Vol. 46, No. 7, 2611–2621, Jul. 2010.
17. Bronn, L., R. J. Wang, and M. J. Kamper, "Development of a shutter type magnetic gear," *Proceedings of the 19th Southern African Universities Power Engineering Conference (SAUPEC)*, 78–82, University of the Witwatersrand, Johannesburg, South Africa, Jan. 28–29, 2010.
18. Faiz, J. and B. M. Ebrahimi, "Mixed fault diagnosis in three-phase squirrel-cage induction motor using analysis of air-gap magnetic field," *Progress In Electromagnetics Research*, Vol. 64, 239–255, 2006.
19. Faiz, J., B. M. Ebrahimi, and M. B. B. Sharifian, "Time stepping finite element analysis of broken bars fault in a three-phase squirrel-cage induction motor," *Progress In Electromagnetics Research*, Vol. 68, 53–70, 2007.
20. Jørgensen, F., T. T. O. Andersen, and P. O. Rasmussen, "The

cycloid permanent magnetic gear," *IEEE Trans. Ind. Appl.*, Vol. 44, No. 6, 1659–1665, Nov./Dec. 2008.

21. Ferreira, C. and J. Vaidya, "Torque analysis of permanent magnet coupling using 2D and 3D finite elements methods," *IEEE Trans. Magn.*, Vol. 25, No. 4, 3080–3082, Jul. 1989.
22. Liu, X., K. T. Chau, J. Z. Jiang, and C. Yu, "Design and analysis of interior-magnet outer-rotor concentric magnetic," *J. Appl. Phys.*, Vol. 105, No. 7, 07F101–7F101-3, Apr. 2009.
23. Evans, D. J. and Z. Q. Zhu, "Influence of design parameters on magnetic gear's torque capability," *2011 IEEE International Electric Machines & Drives Conference (IEMDC)*, 1403–1408, Sheraton Fallsview Hotel & Conference Centre, Niagara Falls, ON, Canada, May 15–18, 2011.
24. Niguchi, N. and K. Hirata, "Cogging torque analysis of magnetic gear," *IEEE Trans. Ind. Electron.*, Vol. 59, No. 5, 2189–2197, May 2012.
25. Niguchi, N., K. Hirata, M. Muramatsu, and Y. Hayakawa, "Transmission torque characteristics in a magnetic gear," *XIX International Conference on Electrical Machines (ICEM)*, 1–6, Rome, Italy, Sep. 6–8, 2010.
26. Furlani, E. P., *Permanent Magnet and Electromechanical Devices,* 207–333, United Kingdom, Sept. 5, 2001.
27. Brovenko, A. V., E. D. Vinogradova, P. N. Melezhik, A. Y. Poyedinchuk, and A. S. Troschylo, "Resonance wave scattering by a strip grating attached to a ferromagnetic medium," *Progress In Electromagnetics Research B*, Vol. 23, 109–129, 2010.